

Dynamic triad interactions and evolving turbulence spectra

Preben Buchhave¹ and Clara M. Velte^{2, a)}¹⁾*Intarsia Optics, Sønderkovvej 3, 3460 Birkerød, Denmark*²⁾*Department of Mechanical Engineering, Technical University of Denmark, Nils Koppels Allé, Building 403, 2800 Kongens Lyngby, Denmark*

(Dated: 16 October 2019)

We investigate the effect of a four-dimensional Fourier transform on the formulation of Navier-Stokes equation in Fourier space and the way the energy is transferred between Fourier components (modal interactions, commonly referred to as triad interactions in the classical 3-dimensional analysis). We specifically consider the effect of a spatially and temporally finite, digitally sampled velocity record on the modal interactions and find that Fourier components may interact within a broadened frequency window as compared to the usual integrals over infinite ranges. We also see how these finite velocity records have a significant effect on the efficiency of the different modal interactions and thereby on the shape and development of velocity power spectra. The observation that mismatches in the wavevector triadic interactions may be compensated by a corresponding mismatch in the frequencies supports the empirically deduced delayed interactions reported in [Josserand *et al.*, *J. Stat. Phys.* (2017)]. Collectively, these results explain the occurrence and time development of the so-called Richardson cascade and also why deviations from the classical Richardson cascade may occur. Finally, we quote results from companion papers that deal with measurements and computer simulations of the time development of velocity power spectra in a turbulent jet flow into which a single Fourier mode (narrow band oscillation) is injected.

I. Introduction

The term triad interaction refers to the elementary momentum interchanges between Fourier components (or other basis functions) of the velocity field in wavevector space. The nonlinear term in Navier-Stokes equation is of the 2nd order and allows only two Fourier components to combine at a time to form a third one. Study of the triad interactions reveals the inner workings of the evolution of the turbulent velocity field and exposes the dynamics of the formation of velocity power spectra.

Most of the literature on the subject of triad interactions¹⁻⁴ describes the ideal case of a homogeneous flow with infinite spatial ranges. The spatial coordinates, \mathbf{r} , and the temporal coordinate, t , would then be coupled through the velocity at each point in the fluid, $d\mathbf{r} = \mathbf{u}(\mathbf{r}, t) dt$.

However, we want to study the turbulent mode interactions in realistic experimental situations. We must then consider a flow with a finite spatial range and a finite time sampled with a finite sampling rate. Moreover, the finite spatial resolution of the measurement volume decouples the spatial and temporal fluctuations of the velocity and forces us to consider the velocity as a stochastic function of four independent parameters – the three spatial coordinates and time. As we shall see, the exception being when Taylor’s hypothesis can be considered a sufficiently accurate approximation for some finite duration in time.

In the current work, we therefore investigate if the time variable has any influence on the triad interactions. The purpose of this work is first and foremost to try to understand the interactions taking place between velocity structures of different scales and to understand the underlying physical pro-

cesses including the effects of realistic flows. At the end, we describe a few experimental and numerical results from two companion papers. In the experimental study⁵, we have investigated this phenomenon by laboratory experiments where a single Fourier mode (narrow band oscillation) is injected into a turbulent flow. In the numerical study⁶ we describe a computer program based on a one-dimensional projection of Navier-Stokes equation, used for illustrating the nonlinear processes. Examples from these studies are quoted at the end of this publication.

It is important in this work to distinguish between the physical velocity that in case of high intensity turbulence consists of velocity structures that fluctuate in space and time and on the other hand the Fourier components that are mathematical plane waves extending over all space and time. In physical space a velocity wave structure cannot retain its shape for long – the high velocity parts will catch up with the low velocity parts, the result being sharpening of the wave front and a generation of higher and higher harmonic frequencies. The tendency of this process to lead to a shock formation is prevented by the dissipation, which removes energy preferentially from the highest frequencies.

By considering realistic digitally sampled velocity signals from finite spatial and temporal ranges, we have gained insight into the temporal development of the interactions between Fourier modes and the efficiency of interactions that are local, where the interacting wave vectors are of similar size, and into non-local interactions, where two wave vectors may be significantly longer than the third. The shape and finite extent of the experimental spatial domain is seen to broaden the peaks of interacting components and to influence the development and shape of the spatial power spectrum by enhancing or suppressing certain interactions.

By including the Fourier transform of the fourth variable in Navier-Stokes equation, namely time, we have succeeded in deriving an expression for the efficiency of triad interactions, be it local or non-local, and in finding expressions for the time

^{a)}Electronic mail: cmve@dtu.dk; <http://www.staff.dtu.dk/cmve> & <http://www.tr1.mek.dtu.dk>

delays in the turbulent cascade process. The time evolution of the spectrum was studied by Josserand *et al.*⁷, who by time correlation methods found cascade delays depending both on the velocity magnitude and the distance between Fourier components.

Previous attempts to derive the importance of local vs non-local triad interactions have considered only the spatial triad interactions². The Richardson cascade³ and the model for the energy transfer in local equilibrium turbulence¹ put forward by Kolmogorov⁴ presumed predominantly local interactions, and phenomena like non-local interactions, localized dissipation and intermittency were not considered important until much later^{8,9}. The question if the energy cascade is primarily caused by local interactions was addressed by Zhou¹⁰ and Grimaji and Zhou¹¹ and recently by analyzing direct numerical simulations (DNS)^{12–14}. The three-dimensional Fourier decomposition is a familiar and fundamental tool for the description of spectral properties. Other bases may be better suited to fluid turbulence such as interactions between helical modes or those that are optimal in the sense of a proper orthogonal decomposition (POD)^{15–20}. However, in this paper we concentrate on Fourier decomposition in a finite spatial and temporal range without loss of generality of the derived results.

That time should be included in the description of the turbulent field in order to capture the full four-dimensional fluctuations of the velocity field and avoid aliasing effects between spatial and temporal fluctuations was already pointed out by W. K. George²¹. In the present work, recognizing the fact that turbulence is a function of both three spatial coordinates and time, we find that the time fluctuations only have a direct effect on the triad interactions in the case of a finite measurement volume and high intensity turbulence. When Taylor's Hypothesis can be invoked, the physical velocity at a measurement point leads to a phase factor increasing linearly with time so the Fourier modes may be considered travelling waves. In this case, the time dependence falls out of the analysis, since no development of the turbulent flow in terms of interactions can take place in an effectively frozen field. However, the spatial triad interactions do not depend on the phase factor, only indirectly on the fluctuating velocity amplitude. Although much literature deals with water waves such as oceanographic waves and coastal waves and connections between their spatial and temporal behavior (e.g. dispersion relations), not much literature can be found on turbulent structures decomposed as traveling waves and possible dispersion relations in wavenumber space.

We begin by exploring the four-dimensional travelling wave Fourier transform. We then consider the effect of real-world signals being sampled digitally and having a finite extent in space and time. Following that, we consider the characteristic time durations of the interactions and the effect of the finite bandwidth on the final shape of the spectrum. Finally, we illustrate our deductions with measured and computer-generated time evolution of velocity power spectra, where a turbulent flow has been seeded with a single, large oscillating mode.

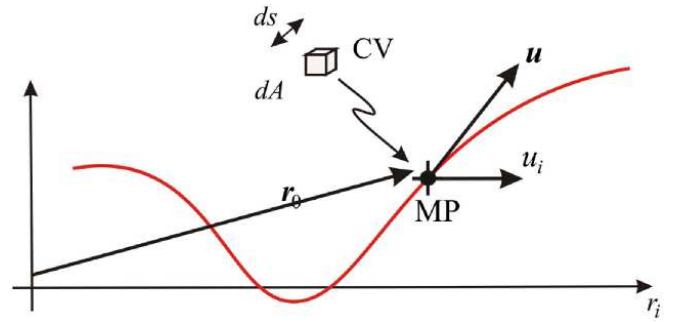


FIG. 1. Fluid control volume CV, instantaneous velocity \mathbf{u} and a component u_i at the CV, a spatial point at position \mathbf{r}_0 and at time, t . The red line indicates the path of a fluid element in time (streak line).

II. Navier-Stokes equation in 4-dimensional Fourier space

It is generally accepted that most constant density and constant viscosity fluid flows are fully described by the Navier-Stokes equation. The Navier-Stokes equation is a momentum conservation equation valid for a continuous, isotropic fluid wherein the Newtonian deformation law reduces to the hydrostatic pressure for zero strain rates, e.g. when the fluid is at rest. The fact that we focus on the Navier-Stokes equation does not make our results and conclusions less general, since the focus is on the non-linear mechanisms, but it simplifies the description of the coupling between shear stresses and strain rates in turbulence modeling.

The Navier-Stokes equation describes the fluid momentum in an infinitesimal control volume in physical space and time. In contrast, the interactions between different scales is most often described in three-dimensional spatial Fourier space^{22,23} using plane waves extending across all space. Herein, we relax these assumptions by including time as an independent variable in the Fourier transform and by delimiting the analyzed flows in space and time.

The nonlinear development of velocity fluctuations is often better described by considering Navier-Stokes equation in the Fourier domain. Here it becomes clear which frequency components interact with each other, what the efficiencies are of these interactions and how they influence the time development of the statistical properties of the turbulent flow, for example the time development of the spatial and temporal velocity power spectra.

To analyze these developments using single-point time-records, we apply the convection record framework²⁴. Figure 1 shows the fluid control volume, $CV = dA \cdot ds$, where dA is the cross-sectional area and ds is the width of the CV in the flow direction.

The Navier-Stokes equation in the physical space coordinate system shown in Figure 1, normalized by setting the density equal to unity, is given by

$$\frac{\partial \mathbf{u}}{\partial t} + (\mathbf{u} \cdot \nabla) \mathbf{u} = -\nabla p + \nu \nabla^2 \mathbf{u} \quad (1)$$

which expresses the momentum change of a fluid element with velocity $\mathbf{u}(\mathbf{r}, t) = (u_1(\mathbf{r}, t), u_2(\mathbf{r}, t), u_3(\mathbf{r}, t))$ where the

position vector $\mathbf{r} = (r_1, r_2, r_3)$ and time is denoted by t . The second term on the left-hand side of the normalized equation represents convective acceleration. The first term on the right-hand side represents the fluctuating force due to pressure and the second the viscous action due to momentum diffusion. We consider constant density flows, which means we can set the divergence of the velocity field equal to zero:

$$\nabla \cdot \mathbf{u} = 0 \quad (2)$$

We can re-write the Navier-Stokes equation in physical space, emphasizing the nonlinear term $\mathbf{N}(\mathbf{r}, t)$:

$$\frac{\partial \mathbf{u}}{\partial t}(\mathbf{r}, t) + \mathbf{N}(\mathbf{r}, t) = -\nabla p(\mathbf{r}, t) + \nu \nabla^2 \mathbf{u}(\mathbf{r}, t) \quad (3)$$

In Fourier space, expanding the classical purely spatial Fourier transform into covering all three spatial dimensions *and* time, the equation becomes

$$-i\omega \hat{\mathbf{u}}(\mathbf{k}, \omega) + \hat{\mathbf{N}}(\mathbf{k}, \omega) = -ik\hat{p}(\mathbf{k}, \omega) - \nu k^2 \hat{\mathbf{u}}(\mathbf{k}, \omega) \quad (4)$$

where $k = |\mathbf{k}|$ for the wave vector $\mathbf{k} = (k_1, k_2, k_3)$, ω denotes temporal frequency and $\hat{\mathbf{N}}(\mathbf{k}, \omega)$ is the Fourier transformed nonlinear term.

Pressure can be eliminated by using the incompressibility condition in Fourier space

$$\mathbf{k} \cdot \hat{\mathbf{u}}(\mathbf{k}, \omega) = 0 \quad (5)$$

to find pressure by solving a Poisson equation over all space. When doing that we see that pressure enters the Navier-Stokes equation in a complicated way, but that the mode interactions are still governed by the same nonlinear term; Taking the divergence of the Navier-Stokes equation (4), we obtain

$$-i\omega \mathbf{k} \cdot \hat{\mathbf{u}}(\mathbf{k}, \omega) + \mathbf{k} \cdot \hat{\mathbf{N}}(\mathbf{k}, \omega) = -ik^2 \hat{p}(\mathbf{k}, \omega) - \nu k^2 \mathbf{k} \cdot \hat{\mathbf{u}}(\mathbf{k}, \omega) \quad (6)$$

where the first and last terms are zero due to continuity. Then

$$\hat{p}(\mathbf{k}, \omega) = \frac{i}{k^2} \mathbf{k} \cdot \hat{\mathbf{N}}(\mathbf{k}, \omega) \quad (7)$$

Inserting the above into the Navier-Stokes equation, we obtain

$$-i\omega \hat{\mathbf{u}}(\mathbf{k}, \omega) + \left[1 - \frac{\mathbf{k}}{k^2}(\mathbf{k} \cdot)\right] \hat{\mathbf{N}}(\mathbf{k}, \omega) = -\nu k^2 \hat{\mathbf{u}}(\mathbf{k}, \omega) \quad (8)$$

where $\frac{\mathbf{k}}{k^2}(\mathbf{k} \cdot)$ is an operator applied onto $\hat{\mathbf{N}}(\mathbf{k}, \omega)$. The first term in the square bracket on the left side is due to convective acceleration and the second one is due to the pressure gradient term, ∇p . It is important to note here, that the effect on both convection and the pressure gradient is governed by the same non-linear term, $\hat{\mathbf{N}}(\mathbf{k}, \omega)$.

Thus, assuming the velocity vector is known, either through measurement, modeling or solution of Poisson's equation with the given boundary conditions, the modal interactions between Fourier components are determined by $\hat{\mathbf{N}}(\mathbf{k}, \omega)$. In the following we therefore proceed by analyzing the effect of $\hat{\mathbf{N}}(\mathbf{k}, \omega)$.

A. 4-dimensional Fourier decomposition with travelling waves

It is therefore sufficient to limit our analysis to consider the nonlinear term $\hat{\mathbf{N}}(\mathbf{k}, \omega)$. We will herein reserve the term 'triad interactions' to the interactions between wavenumber vectors, while the term 'modal interactions' will be used for the more general interactions across wavenumber and frequency.

The 4-dimensional Fourier transform over all space and time is given by

$$\hat{\mathbf{u}}(\mathbf{k}, \omega) = \int \iiint \mathbf{W}(\mathbf{r}) W(t) \mathbf{u}_{\text{homog.}}(\mathbf{r}, t) e^{-i(\mathbf{k} \cdot \mathbf{r} - \omega t)} d\mathbf{r} dt \quad (9)$$

where $\mathbf{W}(\mathbf{r})$ and $W(t)$ are window functions delimiting a finite region of an otherwise homogeneous (infinite) velocity field $\mathbf{u}_{\text{homog.}}(\mathbf{r}, t)$ and time record. The spatially and temporally limited velocity field is denoted $\mathbf{u}(\mathbf{r}, t) = \mathbf{u}_{\text{homog.}}(\mathbf{r}, t) \mathbf{W}(\mathbf{r}) W(t)$ in the derivations that follow. The presence of the window functions reflects the physical reality of a finite region of the velocity field and eliminates the problem of an infinite integral. The shapes of the windows are dependent on the flow geometry and may fluctuate in space and time.

Expanding the velocity field in 4-dimensional Fourier components amounts to an expansion in travelling plane waves (which includes the conventional fixed spatial wave field for $t = \text{constant}$):

$$\mathbf{u}(\mathbf{r}, t) = \frac{1}{(2\pi)^4} \int \iiint e^{i(\mathbf{k} \cdot \mathbf{r} - \omega t)} \hat{\mathbf{u}}(\mathbf{k}, \omega) d\mathbf{k} d\omega, \quad (10)$$

This equation represents the spectral decomposition of the velocity field with $\hat{\mathbf{u}}(\mathbf{k}, \omega)$ being the velocity Fourier components of the spatially and temporally limited field.

The Fourier waves are abstract mathematical concepts, and the physical waves are built up by superposition knowing the values of the Fourier coefficients. Thus, also the triad (or modal) interactions are mathematical concepts. Even so, the strengths of and phase relations between the Fourier coefficients $\hat{\mathbf{u}}(\mathbf{k}, \omega)$ do provide invaluable information about the development of the real physical velocities, $\mathbf{u}(\mathbf{r}, t)$.

Now, consider the spectral representation of the nonlinear convection term, $\hat{\mathbf{N}}(\mathbf{k}, \omega) = FT\{(\mathbf{u}(\mathbf{r}, t) \cdot \nabla) \mathbf{u}(\mathbf{r}, t)\}$:

$$\hat{\mathbf{N}}(\mathbf{k}, \omega) = \int \iiint \mathbf{W}(\mathbf{r}) W(t) e^{-i(\mathbf{k} \cdot \mathbf{r} - \omega t)} d\mathbf{r} dt \times \left[\left(\frac{1}{(2\pi)^4} \int \iiint e^{i(\mathbf{k}_1 \cdot \mathbf{r} - \omega_1 t)} \hat{\mathbf{u}}(\mathbf{k}_1, \omega_1) d\mathbf{k}_1 d\omega_1 \cdot \nabla \right) \frac{1}{(2\pi)^4} \int \iiint e^{i(\mathbf{k}_2 \cdot \mathbf{r} - \omega_2 t)} \hat{\mathbf{u}}(\mathbf{k}_2, \omega_2) d\mathbf{k}_2 d\omega_2 \right] \quad (11)$$

Evaluating the spatial gradients, we obtain:

$$\hat{\mathbf{N}}(\mathbf{k}, \omega) = \int \iiint \mathbf{W}(\mathbf{r}) W(t) e^{-i(\mathbf{k} \cdot \mathbf{r} - \omega t)} d\mathbf{r} dt \times \left[\left(\frac{1}{(2\pi)^4} \int \iiint e^{i(\mathbf{k}_1 \cdot \mathbf{r} - \omega_1 t)} \hat{\mathbf{u}}(\mathbf{k}_1, \omega_1) d\mathbf{k}_1 d\omega_1 \right) \frac{i}{(2\pi)^4} \int \iiint e^{i(\mathbf{k}_2 \cdot \mathbf{r} - \omega_2 t)} \mathbf{k}_2 \cdot \hat{\mathbf{u}}(\mathbf{k}_2, \omega_2) d\mathbf{k}_2 d\omega_2 \right] \quad (12)$$

Collecting the exponentials, we find:

$$\hat{\mathbf{N}}(\mathbf{k}, \omega) = \frac{1}{(2\pi)^4} \int \iiint d\mathbf{k}_1 d\omega_1 \frac{1}{(2\pi)^4} \int \iiint d\mathbf{k}_2 d\omega_2 \times \int \iiint \mathbf{W}(\mathbf{r}) W(t) e^{-i[(\mathbf{k} - \mathbf{k}_1 - \mathbf{k}_2) \cdot \mathbf{r} - (\omega - \omega_1 - \omega_2)t]} d\mathbf{r} dt [(i\mathbf{k}_2 \cdot \hat{\mathbf{u}}(\mathbf{k}_1, \omega_1)) \hat{\mathbf{u}}(\mathbf{k}_2, \omega_2)] \quad (13)$$

Let us analyze the phase of the exponential in the (\mathbf{r}, t) -integral in equation (13) in further detail.

B. Instant vs delayed interactions

As in the classical approach, the nonlinear term could be phase matched if both $\mathbf{k} = \mathbf{k}_1 + \mathbf{k}_2$ and $\omega = \omega_1 + \omega_2$. If the record tends to infinity, the interactions are limited to the product of two delta functions:

$$\delta(\mathbf{k}, \omega) = \delta(\mathbf{k} - \mathbf{k}_1 - \mathbf{k}_2) \delta(\omega - \omega_1 - \omega_2) \quad (14)$$

In this special case, both the wavevectors and the temporal frequencies must be phase matched independently for efficient interactions to occur.

If we can invoke Taylor's Hypothesis during some finite extent in time, e.g. when the turbulence intensity is less than approximately 20%, the time and space fluctuations are coupled through the mean velocity $\mathbf{u}_0 = \mathbf{u}(\mathbf{r}_0, t_0)$; The spatial pattern now moves with a constant velocity and the frequency integral demands the same phase match as the spatial one: $[\omega - (\omega_1 + \omega_2)] \Rightarrow [\mathbf{k} - (\mathbf{k}_1 + \mathbf{k}_2)] \cdot \mathbf{u}_0$. Consequently, the exponential in Equation (13) equals unity.

Thus, we may write the nonlinear term in case of an infinite time and space record using separate phase matches for the spatial and temporal frequencies:

$$\hat{\mathbf{N}}(\mathbf{k}, \omega) = \frac{1}{(2\pi)^4} \int_{\omega_2} \iiint_{\mathbf{k}_2} d\mathbf{k}_2 d\omega_2 [(i\mathbf{k}_2 \cdot \hat{\mathbf{u}}(\mathbf{k} - \mathbf{k}_2, \omega - \omega_2)) \hat{\mathbf{u}}(\mathbf{k}_2, \omega_2)] \quad (15)$$

We can then argue that at a time later, $t_0 + t$, the spatial Fourier transform is unchanged except for a phase factor (the "shift theorem"):

$$\hat{\mathbf{u}}(\mathbf{k}, t) = e^{i\mathbf{k} \cdot \mathbf{u}_0 t} \hat{\mathbf{u}}(\mathbf{k}, t_0),$$

assuming \mathbf{u}_0 nearly unchanged during time t .

Thus, the Fourier components form travelling waves:

$$\hat{\mathbf{u}}(\mathbf{k}, t) = \iiint \mathbf{W}(\mathbf{r}) e^{-i\mathbf{k} \cdot (\mathbf{r} - \mathbf{u}_0 t)} \mathbf{u}(\mathbf{r}, t_0) d\mathbf{r}$$

and the nonlinear term becomes

$$\hat{\mathbf{N}}(\mathbf{k}) = \iiint_{\mathbf{k}_2} (i\mathbf{k}_2 \cdot \hat{\mathbf{u}}(\mathbf{k} - \mathbf{k}_2, (\mathbf{k} - \mathbf{k}_2) \cdot \mathbf{u}_0)) \hat{\mathbf{u}}(\mathbf{k}_2, \mathbf{k}_2 \cdot \mathbf{u}_0) d\mathbf{k}_2 \quad (16)$$

This means that the mode interactions are governed by the conventional spatial triad interactions when Taylor's hypothesis is invoked.

However, the exponent could also become zero if the total argument in the exponential in Equation (13) is zero. Thus, a possible phase mismatch, $\Delta\mathbf{k} \cdot \mathbf{r} = [\mathbf{k} - (\mathbf{k}_1 + \mathbf{k}_2)] \cdot \mathbf{r}$, in the wavevectors could be compensated by a phase mismatch, $\Delta\omega \cdot t = [\omega - (\omega_1 + \omega_2)]t$, in the temporal frequencies. This could happen at a time $t = \Delta\mathbf{k} \cdot \mathbf{r} / \Delta\omega$, if this time will be present within the measured time record. We could call this phenomenon "delayed interactions" or simply describe it as a broadening effect in the spatial interactions caused by the temporal fluctuations. Similar broadening effects of the modal interactions were reported in the works of others⁷.

So, if the turbulence intensity is too high to apply Taylor's

Hypothesis, we see from Eq. (13) that a possible wave vector mismatch can be compensated by a frequency mismatch and vice versa. This means that time fluctuations will broaden the wave vector range of possible modal interactions. Thus, if we assume a temporal bandwidth of, say, $10kHz$, a time delay of $1ms$, and a spatial domain of $0.1m$, then the modal interaction could accept a wave vector mismatch of $\Delta k = t \cdot \Delta\omega/L = 100m^{-1}$.

We can conclude that when turbulence intensity is so high that we cannot speak of a fixed pattern of velocity convecting through a point in space, the ‘‘triade interactions’’ are in reality four-dimensional modal interactions. This implies a broadening of the possible interaction components and the possibility of delayed interactions since the temporal phase shift is time dependent.

III. Digitally sampled finite velocity records

The homogeneous Batchelor turbulence used for theory deductions¹ does not describe a practical experiment. If one were to include homogeneity in time, it would require an infinite record in space and time and the k -vectors must match within delta functions.

For practical signals of finite extent and digital sampling, the situation is somewhat different. If we want to relate to measurements consisting of N samples collected over finite record lengths, L for spatial record length and T for temporal record length, we find that each interaction can take place within a range of wave numbers and frequencies. Let $\Delta k = 1/L$ and $\Delta\omega = 1/T$ be the resolutions in wavenumber and frequency space while $\Delta\lambda = L/N$ and $\Delta t = T/N$ are the resolutions in physical space. It is important to realize that L , T and N are chosen by us to best describe the measurement, but that especially in free flows these limits are hard to define due to the fluctuating nature of the flow boundaries.

In practice, we can estimate L as the maximum extension of a box surrounding the volume of interest, for example with L given by the half width of a jet at the chosen distance from the exit, or as the largest eddy of interest in a particular experiment. T can for example be estimated as the turnover time of the largest eddy of interest.

With for example finite, rectangular windows, the wave vector delta functions are replaced by a product of wave number sinc-functions:

$$\begin{aligned} W_S &= \int_{-L/2}^{L/2} \int_{-L/2}^{L/2} \int_{-L/2}^{L/2} e^{-i(\mathbf{k}-\mathbf{k}_1-\mathbf{k}_2)\cdot\mathbf{r}} d\mathbf{r} \\ &= L^3 \text{sinc}[(\mathbf{k} - (\mathbf{k}_1 + \mathbf{k}_2)) \cdot (\mathbf{r}/|\mathbf{r}|)L/2] \end{aligned} \quad (17)$$

and the frequency delta function by the sinc-function frequency window

$$W_T = \int_{-T/2}^{T/2} e^{-i(\omega-\omega_1-\omega_2)t} dt = T \text{sinc}[(\omega - (\omega_1 + \omega_2))T/2]. \quad (18)$$

These integrals show that interactions may take place not just among the strict (delta function) phase matches, but in

a range of frequencies defined by the width of the sinc-functions, which in turn is defined by the spatial and temporal record lengths.

From $t = \Delta\mathbf{k} \cdot \mathbf{r}/\Delta\omega$, the range of wave numbers can, at least in principle, be related to the frequency range and thereby to the time duration of the interaction if we know the relation between \mathbf{k} and ω , i.e., the dispersion relations for the Fourier waves. However, in a turbulent field there is no known single dispersion relation. Unlike optical waves, for example, fluid velocity waves are unable to form stationary interference patterns. In this respect, they resemble water surface waves that also have velocities very much dependent on wave properties. The interesting thing about velocity waves in turbulence is that they have different velocities independent of the spatial frequencies. In other words, a certain spatial velocity structure, composed of velocity waves, may move with a velocity independent of the structure itself. This, at least, is valid for the small-scale velocity structures.

Thus, the dispersion relation in physical space will depend on the local fluid velocity. This allows us to formulate a dispersion relation $\omega(k) = \mathbf{u}_0 \cdot \mathbf{k}$. So to still be able to advance the analysis, we assume the validity of Taylor’s Hypothesis over a short time period for which we can approximate $u_0 = \Delta\omega/\Delta k$.

In practical situations, we perform measurements by digital sampling. We select the smallest scales of interest, $\lambda_{min} = L/N$ and $\tau_{min} = T/N$ with N being the number of samples. We then apply the discrete Fourier transforms to Eq. (16) and compute the sum

$$\hat{N}(\mathbf{k}, \omega) = \sum_{\mathbf{k}_2=0}^N [(-i\mathbf{k}_2 \cdot \hat{\mathbf{u}}(\mathbf{k} - \mathbf{k}_2, (\mathbf{k} - \mathbf{k}_2) \cdot \mathbf{u}_0)) \hat{\mathbf{u}}(\mathbf{k}_2, \mathbf{k}_2 \cdot \mathbf{u}_0)], \quad (19)$$

where Taylor’s hypothesis is invoked.

The spectral windows resulting from the finite spatial and temporal lengths of the velocity record result in a finite spatial and temporal extent of the interactions. We may define the spatial width of the interaction as the width between the zero crossings of the sinc-function,

$$\Delta k = 4\pi/L.$$

In the same way, the temporal extent may be defined as

$$\Delta\omega = 4\pi/T.$$

We have until now considered the mathematical plane waves making up the basis for the Fourier transform. However, our approach assumes that we know the velocity of the physical waves, $\hat{\mathbf{u}}_0(\mathbf{k}, \omega)$, at the measuring point. We can then use this knowledge to connect the spatial wave to the temporal wave, albeit only for a short time. Knowing \mathbf{u}_0 , we find $\omega = \mathbf{k} \cdot \mathbf{u}_0$ or $\Delta\omega = \mathbf{u}_0 \cdot \Delta\mathbf{k}$. We can then estimate the time duration of the interaction by the Fourier uncertainty as $\Delta t \propto \frac{2\pi}{\mathbf{u}_0 \cdot \Delta\mathbf{k}}$, expressed by the wavenumber range. We find that the duration of the interaction is inversely proportional to the wavenumber span and also depends on the instantaneous wave velocity.

As an example, assume $\Delta k = 10^3 m^{-1}$ corresponding to a $1mm$ wavelength, moving with a velocity $u = 1ms^{-1}$ and

assuming validity of Taylor's Hypothesis, then $\Delta t = \frac{1}{u\Delta k} = \frac{2\pi}{1 \cdot 10^3} = 6.28 \cdot 10^{-3} s$. Thus, a typical interaction lasts a few milliseconds. This agrees with the measurements in Josserand *et al.*⁷.

Thus, the modal interaction time, in addition, of course, depending on the velocity magnitude, also depends on the spatial extent of the measurement region and the resolution in the wavenumber decomposition.

IV. Dynamic evolution of turbulence spectra

The realization that real experiments take place in a limited spatial and temporal region and not in an infinite domain has further consequences for the modal interaction processes and the shape of the spectrum: The spectral windows will influence the efficiency of the interaction between the spectral components.

The efficiency of an interaction between two spectral components will depend both on the spatial extent of the wave overlap and the time duration of the interaction. As we shall show below, the requirement of a good spatial overlap between the waves will enhance interactions between close frequency components (local interactions), but in some cases extended time duration of an interaction may allow also non-local interactions to play a significant role.

These descriptions can also be useful in understanding the technologically and scientifically interesting case of how non-equilibrium turbulence develops downstream of fractal grids^{25,26}. The multiple, but sometimes widely separated (in wavenumber), scales that are introduced simultaneously have a high degree of temporal overlap since they are introduced into approximately the same convection velocity. The energy exchange between components and the dynamic evolution of the spectra can thereby be further accelerated and will also depend directly on the distribution of scales (spatial overlap) introduced by the chosen fractal mesh scales and how efficiently they exchange energy. As opposed to the classical single scale injecting meshes, the fractal grids can thus produce turbulence that develops significantly faster.

In a high Re-number homogeneous turbulence, the spatial and temporal spectral ranges are very large and the spatial and temporal pulse widths correspondingly small. Thus, local interactions will be favored, while the possibility of interactions between widely different scales, non-local interactions, will be small. The efficiency, however, does not require the magnitudes of \mathbf{k}_1 and \mathbf{k}_2 to have the same size as \mathbf{k} . This can explain the phenomenon observed from DNS computations sometimes denoted "local transfer by non-local interaction"²⁷, where efficient interaction occurred even when \mathbf{k}_1 and \mathbf{k}_2 were much greater than \mathbf{k} . In special circumstances, e.g. in thin shear layers or near large vortices, the interaction may persist for a longer time, and non-local interactions may be important in those cases. Examples with clear deviations from the Richardson cascade are available^{28–30} and an extensive review of observations of non-classical and so-called inverse cascades is presented in available work³¹.

This section will therefore first detail the modal interaction

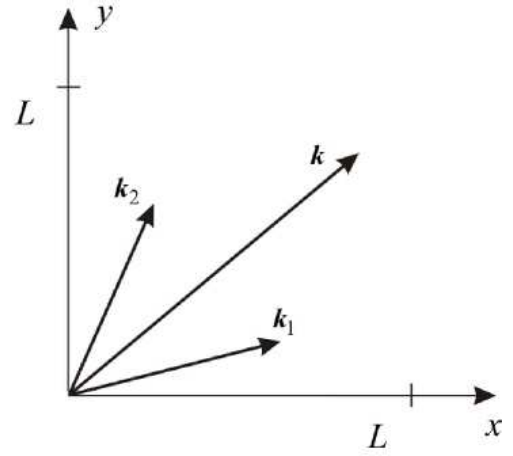


FIG. 2. Wave vectors for three interacting Fourier components (plane waves) in the spatial domain $L \times L$.

efficiency and the dependency upon temporally and spatially finite flows. The impact of the cascaded delays and the implications for the time evolution of spectra will thereafter be discussed. Finally, supporting experiments and simulations are shown to illustrate these effects in a real flow setting and as simulated directly from the Navier-Stokes equation.

A. Modal interaction efficiency – effects of spatially finite flows

Consider as a simple example the interaction between two physical plane velocity waves limited to an experiment region L^3 by rectangular windows in space and T in time. Those two physical waves will be represented in frequency space by a range of infinite plane waves. If we pick one pair of Fourier components, \mathbf{k}_1 and \mathbf{k}_2 , we see that they together with \mathbf{k} define a plane. In this 2D plane, the overlap between two complex plane waves, with different wavenumbers and propagation directions, in a physical domain $L \times L$, is given by:

$$\begin{aligned} \eta_S &= \int_{-L/2}^{L/2} \int_{-L/2}^{L/2} e^{i\mathbf{k}_1 \cdot \mathbf{r}} e^{i\mathbf{k}_2 \cdot \mathbf{r}} dx dy \\ &= \int_{-L/2}^{L/2} e^{i[k_1 \cos \theta_1 + k_2 \cos \theta_2]x} dx \cdot \int_{-L/2}^{L/2} e^{i[k_1 \sin \theta_1 + k_2 \sin \theta_2]y} dy \\ &= L^2 \text{sinc} \left[(k_1 \cos \theta_1 + k_2 \cos \theta_2) \frac{L}{2} \right] \cdot \\ &\quad \text{sinc} \left[(k_1 \sin \theta_1 + k_2 \sin \theta_2) \frac{L}{2} \right] \end{aligned}$$

where θ_1 and θ_2 are the angles of the respective wavenumber vectors to the x-axis.

Within a close range defined by the sinc-functions, the waves interact efficiently. This is plotted in Figure 3 with a fixed value of \mathbf{k}_1 , and with \mathbf{k}_2 varying. N is the number of modes or frequencies in the Fourier expansion, for example $N = 200$. The other values for the plot are $k_1 = |\mathbf{k}_1| = 10$ and

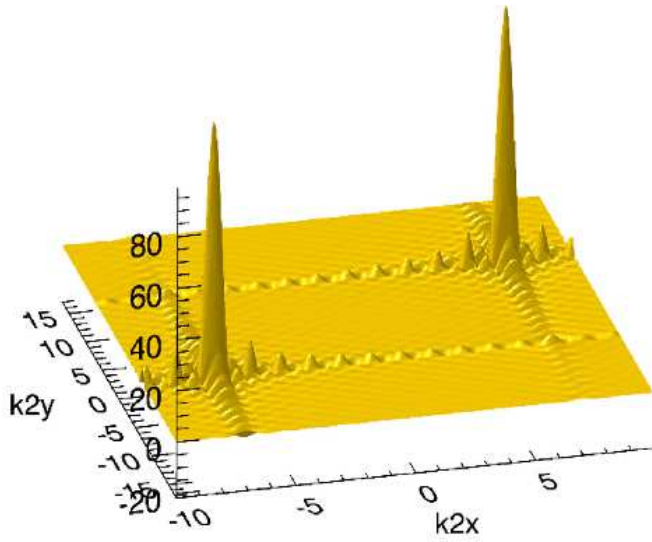


FIG. 3. Overlap integral as a function of \mathbf{k}_2 for a fixed value of \mathbf{k}_1 .

$\theta_1 = \pi/3$. $k_2 = |\mathbf{k}_2|$ varies from -20 to 20 and θ_2 varies from 0 to 2π . The peak in the fourth quadrant occurs because \mathbf{k} -vectors pointing in the opposite direction have the same overlap as the ones in the first quadrant. Figure 3 also shows that the interaction efficiency is not limited to the center-lobe, but spreads across the higher order lobes over large distances from the center lobe.

If Taylor's frozen field hypothesis applies, where the waves move at the same speed, the overlap efficiency (Figure 3) as a result also remains stationary over time. In the case that Taylor's hypothesis does not apply, e.g. in high intensity turbulence, the wave speeds will differ and the interactions will be time limited. In this case, the pattern in Figure 3 will change intermittently with time.

We notice that the width of the wave number uncertainty, Δk_x , defined by the zero crossings of the sinc-function $\Delta k_x L/2 = 2\pi$, depends on the interaction area side length, L . The effect on the turbulence power spectrum by this spectral window is illustrated in Figure 4, which compares a computer simulation with and without the effect of the finite interaction area. The suppression of odd numbered 'harmonics', as observable from Figure 4b, will be explained in the following.

B. Cascaded delays – time evolution of spectra

In equation (13) it was established that the potential mismatch between spatial and temporal frequencies allowed for delays to occur in the interactions. Each interaction thus develops with a characteristic time, which depends both on the magnitude of the Fourier components, the spectral bandwidth and the overlap efficiency factor resulting from the finite experimental region.

However, the interaction time also depends on the number of time steps needed to go from \mathbf{k}_1 and \mathbf{k}_2 to \mathbf{k} in equation

(13). Thus, the number of delays in each modal interaction is proportional to $1 + |j_1 - j_2|$, where the initial constant 1 accounts for the first interaction process and j_1 and j_2 are two wavenumber indices (integers) for the wave vectors interacting to produce the resulting (third) peak in wavenumber space.

The cascaded delay in time is proportional to the sum of time delays. Let us give a couple of examples, where we consider individual modal interactions in k -space. We consider the presence of only one spatial input frequency component, k_0 , and look at a few simple cascade processes for the formation of harmonics. Three different low order cascade processes are illustrated in Figure 5.

Frequency doubling: $k_0 \Rightarrow 2k_0$

In this example, $k_1 = k_2$ and there is only one delay, $1 + |j_1 - j_2| = 1$.

Frequency tripling: $k_0 + 2k_0 \Rightarrow 3k_0$

Here $k_1 = k_0$ and $k_2 = 2k_0$. Thus $1 + |j_1 - j_2| = 2$. But $k_2 = 2k_0$ must be created first resulting in a total cascade delay of 3. Moreover, in a realistic situation, k_1 and k_2 would be quite different in size, resulting in a less efficient spatial overlap and interaction (see section on modal efficiency factor).

Frequency quadrupling: $2k_0 + 2k_0 \Rightarrow 4k_0$

Here $k_1 = 2k_0$ and $k_2 = 2k_0$. $j_1 = j_2$, so there is only one delay in this interaction, $1 + |j_1 - j_2| = 1$. But $2k_0$ must be created first, resulting in a total cascade delay of 2.

Thus, the fourth harmonic would be created earlier and more efficiently than the third harmonic. The resulting suppression of the third (and other odd) harmonics in relation to the even ones, as described here, is clearly visible in Figure 4b.

It should be noted here, that the actual processes are difficult to isolate and that experiments to unveil these processes therefore are often sensitive to experimental conditions, such as initial and boundary conditions (which are also well-known properties for the differential equations that govern the flow). Other effects that further complicate the interactions are the multiple lobes in the window-function, the fact that the window function in general is not rectangular and that the window is likely to fluctuate wildly in time and space. Nevertheless, we have been able to isolate this effect to a reasonable degree and observe the developments of the delayed interactions, as described in more detail in the following section.

C. Experiments and numerical simulations

Our simple analysis allows us to estimate the duration of individual modal interaction processes and the total delay in a process involving a number of cascade steps. We have illustrated these results in two ways that we shall publish separately. In one study⁵, we measured the development of the velocity power spectrum using a hot-wire anemometer in the laminar core of a large free jet in air into which we injected a single large mode upstream. By measuring the power

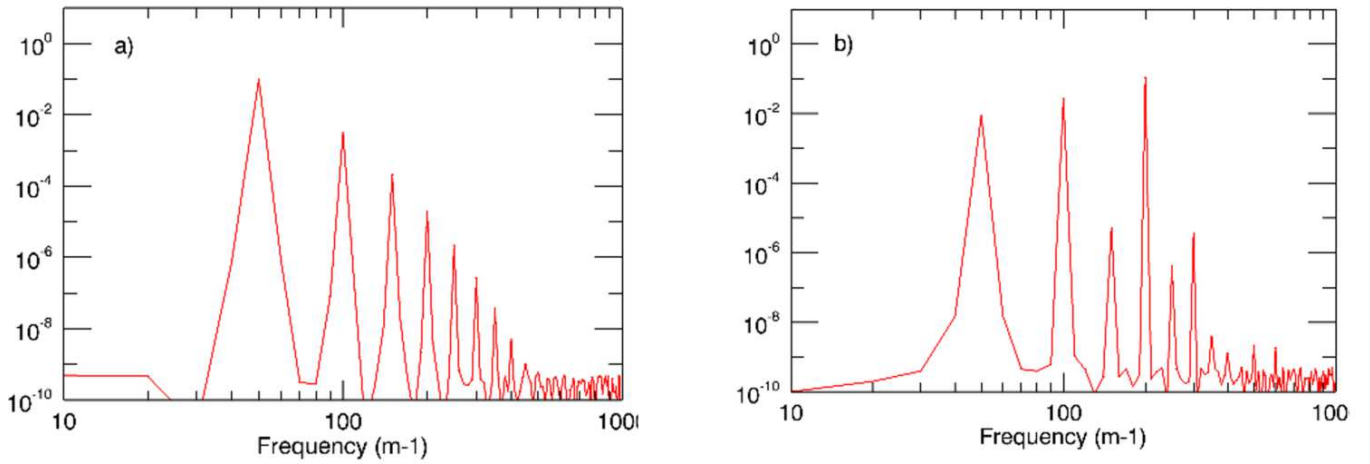


FIG. 4. Computer simulation of the development of the spectrum of an initial signal consisting of a single spatial frequency of 50 m^{-1} . Figure 4(a): Large interaction volume, high spatial bandwidth which does not interfere with the conversion efficiency. Figure 4(b): Small interaction volume, the sinc-function spectral window reduces conversion to odd orders.

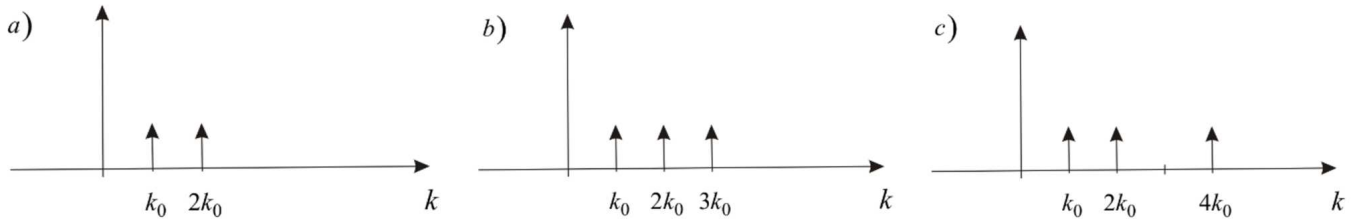


FIG. 5. (a) Frequency doubling. (b) Frequency tripling. (c) Frequency quadrupling.

spectrum at several downstream locations, we could follow the time development of the spectrum and the appearance of the first higher harmonics generated by the nonlinear term in Navier-Stokes equation.

In one case, see Figures 6 and 7, we used vortex shedding behind a rod with a rectangular cross-section placed across the jet to inject a narrow band oscillation which can represent a single oscillating mode close to the jet exit. The jet exit had a contraction ratio of $2.4 : 1$ and an exit diameter of 100 mm . The jet was run at a jet exit velocity of 1.6 m s^{-1} . This produced a sufficiently large laminar jet core to be able to serve well as an open wind tunnel test section. The rectangular rod had a cross-section of $2\text{ mm} \times 10\text{ mm}$ and thus significantly smaller dimensions than the jet exit. The rod length was 300 mm , corresponding to three jet exit diameters and the rod was placed to cover with good margin the jet nozzle extent across the exit diameter. The rod was positioned 1 mm from the nozzle and across the jet exit so that it was passing through the jet centerline. The sharp edges of the rectangular cross-section enabled vortex shedding with a sufficiently distinct base frequency to be able to trace the downstream development of the first and subsequent harmonics. This effect turned out to be most distinguishable in the measurements when the longest dimension (10 mm) of the rod cross section was aligned with the jet centerline. A single component hot-wire with a PicoScope to monitor the live frequency con-

tent development were used to select the optimal flow setting, measurement positions and to acquire the end result. This resulted in acquisition of the above described flow setting in ten points along the downstream direction with 1 mm spacing, of which only the downstream positions 1 mm , 5 mm and 10 mm are shown herein. The most upstream measurement point was placed 0.5 mm to the side away from the edge and the wake of the rod, see Figure 6. Further detail about this experiment can be found openly available⁵.

The first spectrum, Figure 7a, shows the measured power spectrum 1 mm downstream from the rod where only the fundamental oscillation is present. Figure 7b shows the spectrum 5 mm downstream and Figure 7c the spectrum 10 mm downstream. 100 measured spectra have been averaged for each downstream position. Knowing the velocity as a function of downstream position, we can calculate the convection time and thereby find the time history for the modal interactions⁵.

In a second paper⁶, we show results of a computer calculation of a one-dimensional projection of Navier-Stokes equation. We have implemented a one-dimensional version of Navier-Stokes equation²⁴ in a program that can be executed on a laptop PC in a few hours. By neglecting the direction of the velocity vector and only considering the velocity magnitude at a point as a function of time, the system of equations reduces to one dimension so that it is numerically solvable. The one-dimensional solution allows us to compute the

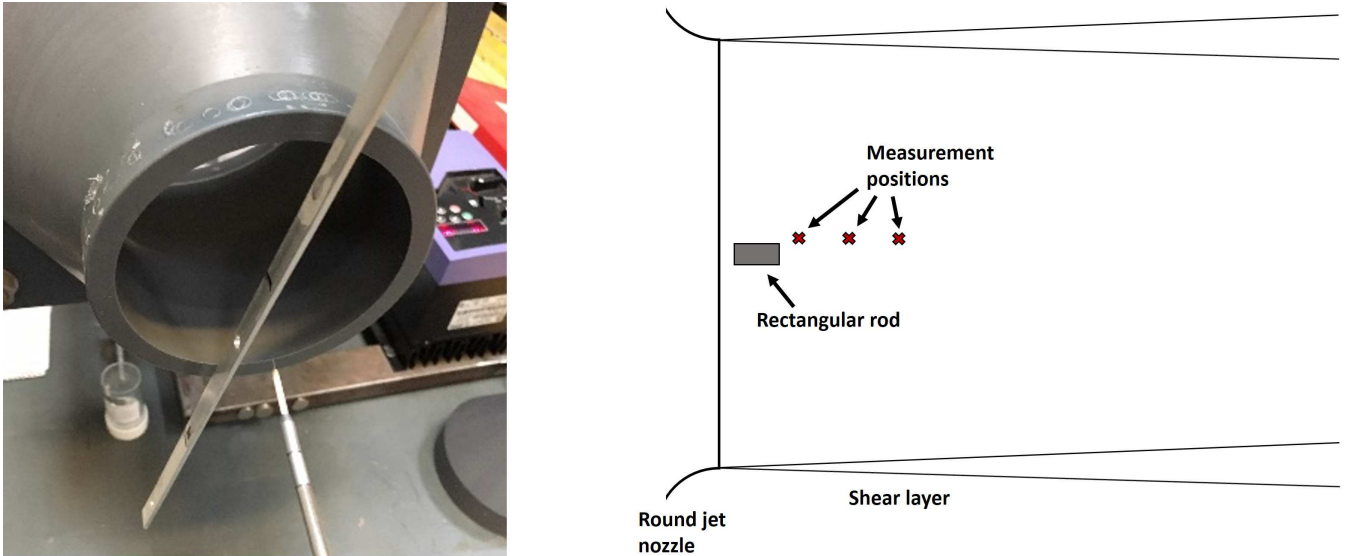


FIG. 6. (Left) Picture and (Right) sketch of the simple experimental setup used to isolate the interactions resulting from a distinct frequency shed off from a rectangular rod. The jet was large compared to the rod, such that the laminar core of the jet could create an environment similar to an open wind tunnel test section. A single component hot-wire (as seen in the left figure) was used to trace the downstream development from the initial single frequency injected by the rectangular rod.

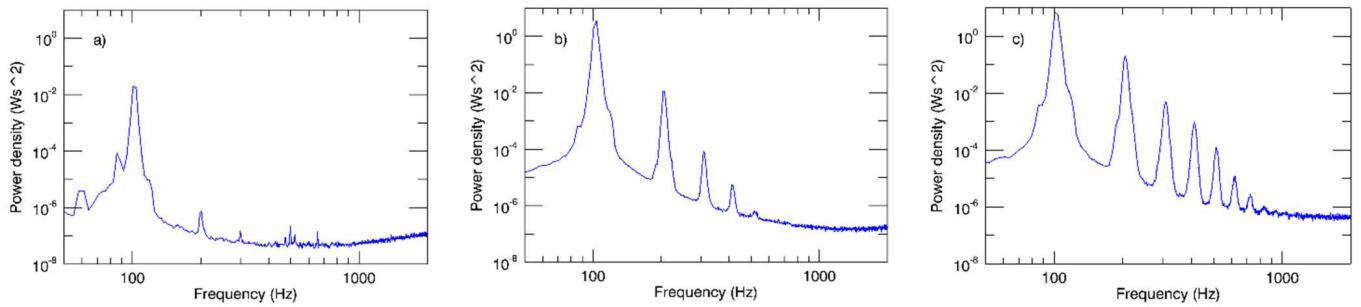


FIG. 7. Measured velocity power spectra with increasing downstream positions from left to right. a) 1 mm, b) 5 mm and c) 10 mm downstream, respectively.

kinetic energy and the turbulent structure functions directly from Navier-Stokes equation without any additional assumptions except for the pressure term, which would require either a full three-dimensional solution for the whole flow field or a model for the pressure fluctuations²⁴. We are, among many other things, able to simulate the time development of a velocity power spectrum consisting of a low intensity von Kármán-type turbulence to which we added a single low frequency mode.

In Figure 8 we show the development of a single Fourier mode in the same laminar jet core flow as described above and in Figure 6 and 7. Instead of a computer-generated oscillating time trace we used the time trace actually measured near the rod (the same position and same velocity trace as in Figure 7a) and processed the downstream development of this time trace using our Navier-Stokes simulator.

Thus, the first plot should be identical to the measured one. (The slight differences in the initial spectra are due to the somewhat different filter settings and window functions of the

PicoScope used for the measured spectra and the fast Fourier transform (FFT) settings used for the computations). The following plots show the velocity power spectrum computed by the Navier-Stokes simulator based on an average of 20 measured time traces. This should be held up against the ones measured downstream where the convection time has allowed the flow to develop. One clearly sees the effect of the cascaded delays on the development of the spectrum and the sequence of appearance of the first harmonics.

V. Conclusions

We studied the modal interactions between the Fourier components of a full four-dimensional Fourier transform of a turbulent velocity field including both the three spatial coordinates and time. We have analyzed various forms of the resulting phase factor in the 4-dimensional Fourier transform

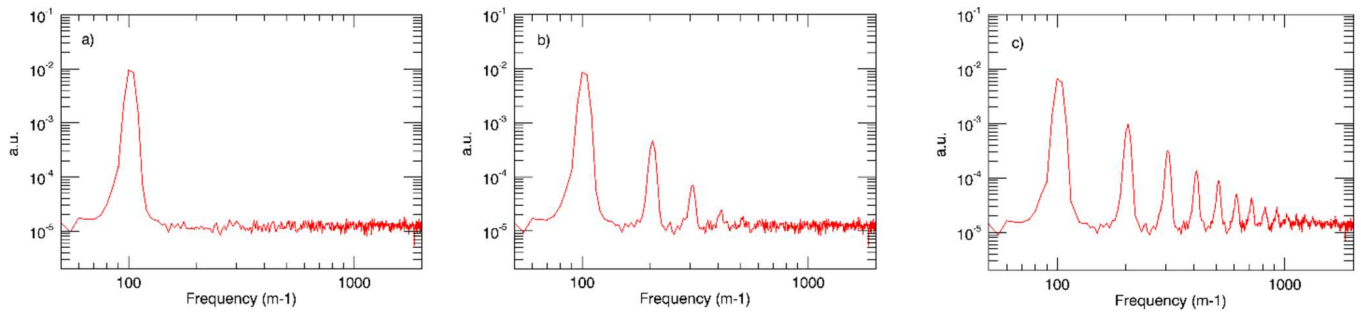


FIG. 8. Computed velocity power spectra with increasing time from left to right. The downstream development times have been chosen to approximately match the downstream developments displayed in Figure 7.

and the effect on the modal interactions. In this process, we found that time must be considered an independent variable when Taylor's frozen field hypothesis does not apply or when the finite probe volume decouples time and space in the otherwise valid definition $\mathbf{u}(\mathbf{r}, t) = d\mathbf{r}/dt$.

The flow was then assumed to be confined to a limited spatial region and a finite time record to illustrate a realistic flow situation. We found that time plays a direct role in the triad interactions in cases where Taylor's frozen field hypothesis is not valid. However, when the field can be regarded as frozen, the description returns to the original pure spatial one.

In cases where Taylor's hypothesis is not applicable, the fluctuating temporal phase can compensate for a spatial phase mismatch and through that effect broaden the phase match condition. The finite spatial and temporal domain in itself creates a spectral window for the modal interactions, again introducing a spectral broadening effect. Furthermore, the limited spatial domain influences the efficiency of the Fourier component overlap, which alters the shape of the generated spectrum. The dynamic evolution of the spectra was illustrated in that each interaction process must precede the next with an associated delay. Experiments and simulations lend strong support for this as well.

Finally, we quoted some results from two companion papers. These examples show good agreement between a measurement in a free jet in air into which a single Fourier component is injected, for instance by vortex shedding, and a computation of the time development of the same velocity time trace by a simplified one-dimensional projection of the terms in Navier-Stokes equation onto the instantaneous velocity direction.

These investigations have resulted in a better understanding of modal interactions and illustrated the processes participating in the non-linear interactions and energy transfer between scales in turbulence generation and decay.

Acknowledgments

The authors wish to thank Professor Emeritus Poul Scheel Larsen for many helpful discussions. We also wish to acknowledge the generous support of Fabriksejer, Civilingeniør Louis Dreyer Myhrwold og hustru Janne Myhrwolds Fond

(Grant Journal No. 13-M7-0039 and 15-M7-0031), and Reinholdt W. Jorck og Hustrus Fond (Grant Journal No. 13-J9-0026). The final stages of the project would not have been possible without the support of the European Research Council: This project has received funding from the European Research Council (ERC) under the European Union's Horizon 2020 research and innovation programme (grant agreement No 803419).

Bibliography

- ¹G. K. Batchelor. In *The Theory of Homogeneous Turbulence*. Cambridge University Press, 1953.
- ²Robert H. Kraichnan. The structure of isotropic turbulence at very high Reynolds numbers. *Journal of Fluid Mechanics*, 5:497–1959.
- ³Lewis Fry Richardson. In *Weather prediction by numerical process*. Cambridge Univ. Press, 1922.
- ⁴Andrey N. Kolmogorov. The local structure of turbulence in incompressible viscous fluid for very large Reynolds numbers. *Proc. R. Soc. Lond. A*, 434:9–13, 1991. DOI: 10.1098/rspa.1991.0075.
- ⁵Margherita Dotti, Rasmus Korslund Schlander, Preben Buchhave, and Clara M. Velte. Experimental investigation of the turbulent cascade development in time by injection of single large-scale Fourier modes. *under review in Journal of Turbulence*, arXiv:1908.05613 [physics.flu-dyn];–, 2019.
- ⁶Preben Buchhave, and Clara M. Velte. A 1D Navier-Stokes Machine and its application to turbulence studies. *under preparation for Journal of Turbulence*, pages –.
- ⁷Christophe Josserand, Martine Le Berre, Thierry Lehner, and Yves Pomeau. Turbulence: Does Energy Cascade Exist? *Journal of Statistical Physics*, 10.1007/s10955-016-1642-5 and 10.1007/10955.1572-9613:596–625, 2017.
- ⁸Andrey N. Kolmogorov. A refinement of previous hypotheses concerning the local structure of turbulence in a viscous incompressible fluid at high Reynolds number. *Journal of Fluid Mechanics*, 13:82–85, 1962. DOI: 10.1017/S0022112062000518.
- ⁹John Christos Vassilicos. In *Intermittency in Turbulent Flows*. Cambridge Univ. Press, 2000.
- ¹⁰Ye Zhou. Interacting scales and energy transfer in isotropic turbulence. *Physics of Fluids A: Fluid Dynamics*, 5:2511, 1993. <https://doi.org/10.1063/1.858764>.
- ¹¹Sharath S. Girimaji and Ye Zhou. Spectrum and energy transfer in steady Burgers turbulence. *Physics Letters A*, 202:279–287, 1995. [https://doi.org/10.1016/0375-9601\(95\)00317-V](https://doi.org/10.1016/0375-9601(95)00317-V).
- ¹²Gerrit E. Elsinga and Ivan Marusic. The anisotropic structure of turbulence and its energy spectrum. *Physics of Fluids*, 28:011701, 2016.
- ¹³Jonasz Słomka, Piotr Suwara, and Jörn Dunkel. The nature of triad interactions in active turbulence. *Journal of Fluid Mechanics*, 841:702–731, 2018.

- ¹⁴Wang Bo-Bin, Cui Gui-Xiang, Xu Chun-Xiao, and Zhang Zhao-Shun. The Similarity of Non-local Triad Interactions in Energy Transfer of Isotropic Turbulence. *Chinese Physics Letters*, 29, 2012.
- ¹⁵Thomas S. Lundgren. Strained spiral vortex model for turbulent fine structure. *Physics of Fluids*, 25:2193, 1982.
- ¹⁶Fabian Waleffe. The nature of triad interactions in homogeneous turbulence. *Physics of Fluids*, 4:350, 1992.
- ¹⁷Ganapati Sahoo and Luca Biferale. Energy cascade and intermittency in helically decomposed Navier–Stokes equations. *Fluid Dynamics Research*, 50, 2018.
- ¹⁸Azur Hodžić. In *A Tensor Calculus Formulation of the Lumley Decomposition applied to the Turbulent Axi-symmetric Jet Far-field*. PhD Dissertation, Technical University of Denmark, Kgs. Lyngby, Denmark, 2019.
- ¹⁹Azur Hodžić, Knud Erik Meyer, Clara M. Velte, and William K. George. Lumley Decomposition of the Turbulent Round Jet Far-field. Part 1 – Kinematics. *submitted to Journal of Fluid Mechanics*, *arXiv:1908.05134 [physics.flu-dyn]*.
- ²⁰Azur Hodžić, Knud Erik Meyer, William K. George, and Clara M. Velte. Lumley Decomposition of the Turbulent Round Jet Far-field. Part 2 – Dynamics. *submitted to Journal of Fluid Mechanics*, *arXiv:1909.01307 [physics.flu-dyn]*.
- ²¹William K. George. A 50-Year Retrospective and the Future. In *Whither Turbulence and Big Data in the 21st Century?*, pages 13–48. Springer Verlag, 2017. Editors: Andrew Pollard, Luciano Castillo, Luminita Danaila, Mark Glauser.
- ²²P. K. Yeung and James G. Brasseur. The response of isotropic turbulence to isotropic and anisotropic forcing at the large scales. *Physics of Fluids A*, 3:884897, 1991. <https://doi.org/10.1063/1.857966>.
- ²³P. K. Yeung, James G. Brasseur, and Qunzhen Wang. Dynamics of direct large-small scale couplings in coherently forced turbulence: concurrent physical- and Fourier-space views. *Journal of Fluid Mechanics*, 283:43–95, 1995. <https://doi.org/10.1017/S0022112095002230>.
- ²⁴Preben Buchhave and Clara M. Velte. Measurement of turbulent spatial structure and kinetic energy spectrum by exact temporal-to-spatial mapping. *Physics of Fluids*, 29:085109, 2017. <https://doi.org/10.1063/1.4999102>.
- ²⁵P. C. Valente and J. C. Vassilicos. The energy cascade in grid-generated non-equilibrium decaying turbulence. *Physics of Fluids*, 27:045103, 2015. <https://doi.org/10.1063/1.4916628>.
- ²⁶Koji Nagata, Teppei Saiki, Yasuhiko Sakai, Yasumasa Ito, and Koji Iwano. Effects of grid geometry on non-equilibrium dissipation in grid turbulence. *Physics of Fluids*, 29:015102, 2017. <https://doi.org/10.1063/1.4973416>.
- ²⁷Wang Bo-Bin, Cui Gui-Xiang, Xu Chun-Xiao, and Zhang Zhao-Shun. The Similarity of Non-local Triad Interactions in Energy Transfer of Isotropic Turbulence. *Chinese Physics Letters*, 29, 2012.
- ²⁸A. Sozza, G. Boffetta, P. Muratore-Ginanneschi, and S. Musacchio. Dimensional transition of energy cascades in stably stratified forced thin fluid layers. *Physics of Fluids*, 27:035112, 2015. <https://doi.org/10.1063/1.4915074>.
- ²⁹Antoine Campagne, Basile Gallet, and Frédéric Moisy. Direct and inverse energy cascades in a forced rotating turbulence experiment. *Physics of Fluids*, 26:125112, 2014. <https://doi.org/10.1063/1.4904957>.
- ³⁰D. Oks, P. D. Mininni, R. Marino, and A. Pouquet. Inverse cascades and resonant triads in rotating and stratified turbulence. *Physics of Fluids*, 29:111109, 2017. <https://doi.org/10.1063/1.5001740>.
- ³¹A. Pouquet, R. Marino, P. D. Mininni, and D. Rosenberg. Dual constant-flux energy cascades to both large scales and small scales. *Physics of Fluids*, 29:111108, 2017. <https://doi.org/10.1063/1.5000730>.
- ³²R. H. Kraichnan. The structure of isotropic turbulence at very high Reynolds numbers. *Journal of Fluid Mechanics*, 5:497–543, 1959. <https://doi.org/10.1017/S0022112059000362>.
- ³³J. Lee. Dynamical behavior of the fundamental triad-interaction system in three-dimensional homogeneous turbulence. *Physics of Fluids*, 22, 1979. <https://doi.org/10.1063/1.862433>.
- ³⁴J. G. Brasseur and C.-H. J. WeiLee. Interscale dynamics and local isotropy in high Reynolds number turbulence within triadic interactions. *Physics of Fluids*, 6, 1994. <https://doi.org/10.1063/1.868322>.